# Dependence on pulse duration and foil thickness in high-contrast-laser proton acceleration

A. Flacco,[1] F. Sylla,[1] M. Veltcheva,[1,2] M. Carrié,[3] R. Nuter,[3] E. Lefebvre,[3] D. Batani,[2] and V. Malka[1]
[1]*Laboratoire d'Optique Appliquée, ENSTA–ParisTech, École Polytechnique-ParisTech, CNRS UMR 7639, Chemin de la Huniére, 91761 Palaiseau Cedex, France*
[2]*Dipartimento di Fisica "G. Occhialini," Università degli Studi di Milano-Bicocca, Piazza della Scienza 3, 20126 Milano, Italy*
[3]*CEA, DAM, DIF, 91297 Arpajon, France*

(Received 23 March 2009; revised manuscript received 9 December 2009; published 11 March 2010)

Experimental measurements of proton acceleration with high intensity and high-contrast short laser pulses have been carried out over an order of magnitude range in target thickness and laser pulse duration. The dependence of the maximum proton energy with these parameters is qualitatively supported by two-dimensional particle-in-cell simulations. They evidence that two regimes of proton acceleration can take place, depending on the ratio between the density gradient and the hot electron Debye length at the rear target surface. As this ratio can be affected by the target thickness, a complex interplay between pulse duration and target thickness is observed. Measurements and simulations support unexpected variations in the laser absorption and hot electron temperature with the pulse duration and laser intensity, for which density profile modification at the target front surface is the controlling parameter.

DOI: 10.1103/PhysRevE.81.036405 PACS number(s): 52.38.Kd

Energetic proton and ion beams, resulting from the interaction of laser pulses at relativistic intensities ($I > 10^{18}$ W/cm$^2$) with thin foil targets, have been reported in many studies [1–3]. Laser-accelerated proton beams show a half divergence of $\approx 10°$, decreasing for higher energies, and a good laminarity [4,5].

During the interaction, the laser energy is primarily transferred to electrons in the target, accelerated to relativistic energies. The extraction and acceleration of ions is a consequence of the charge separation that is set between this hot electron component and the cold ions at the plasma/vacuum interface. This mechanism (TNSA [6,7], Target Normal Sheath Acceleration) has been extensively studied and is the source of the most energetic protons produced in the process [8,9]. The study of the accelerated protons also gives an insight on the interaction of relativistic intensity laser pulses with solid targets.

In experiments, the laser prepulse or Amplified Spontaneous Emission (ASE) pedestal affects the target surface and therefore the absorption of laser energy, the distribution of hot electrons and, in some cases, the conditions at the target rear surface. The pedestal interacts with the target on a nanosecond time scale before the ultrahigh intensity peak; its energy ionizes the illuminated surface and a density gradient is produced. This preplasma is known to affect the various mechanisms involved in the energy deposition process [10–12]; in previous studies it has been shown that a plasma density gradient can be beneficial to laser energy absorption [13,14]. On the other hand, a shock wave launched by the prepulse into the target can trigger the early expansion of the nonilluminated surface, where the TNSA process takes place: the evolution of a density gradient on the back surface has been proven to be detrimental to the acceleration process, decreasing the maximum proton energy [15–17]. Higher proton energies are usually reached with thinner targets, for hot electrons are less dispersed while drifting to the accelerating surface, thus resulting in a higher charge density. Nevertheless, thinner targets are also more easily destroyed by shock effects associated to the interaction with the pedestal. The two competing phenomena are responsible for the existence of an optimal target thickness [18,19] for given laser parameters.

The dependence of the acceleration process on the laser pulse duration has been addressed in several works, both through fluid [20,21] and analytical [22] models, kinetic simulations [23], and experimental results [24,25]. For instance, it has been suggested [18,26,27] that the time over which the protons are accelerated is related to the laser pulse duration, since during this time the hot electron temperature $T_{\mathrm{hot}}$ is kept constant by the sustaining action of the laser field. If $L_{\mathrm{target}}/c < \tau_L$, $L_{\mathrm{target}}$ being the target thickness and $\tau_L$ the laser pulse duration, it has been also suggested [24] that the hot electron density is enhanced by multiple round trips through the target during the laser action.

The measurement of the correlation between the laser pulse duration and proton acceleration is made difficult by the presence of the laser pedestal. The last developments in laser technology enable the production of contrast ratios as high as $I_0/I_{\mathrm{ASE}} > 10^9$: this allows the use of thinner targets, thus increasing the maximum proton energy. High-contrast laser sources provide the user with cleaner and more controllable interaction conditions. The use of high-contrast laser pulses in ion acceleration experiments showed unprecedented results [19,28], deepening the insight on the acceleration mechanisms and underlining the importance of a precise control of the interaction parameters.

In this paper, we investigate the effect of the laser pulse duration on the proton acceleration process for different target thicknesses, using a high-contrast laser beam. In previous studies, the dependence of laser absorption and electron temperature with pulse duration and intensity were derived from past measurements under poor contrast conditions. The present work, associating experimental measurements and detailed simulation analysis, clearly demonstrates that new scalings must be accounted for under conditions of high laser contrast.

The experiments have been performed on the *Salle Jaune* multiterawatt laser facility at the *Laboratoire d'Optique Ap-*

 

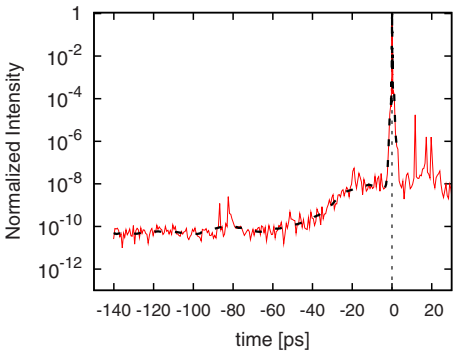


FIG. 1. (Color online) Cross-correlation ($3\omega$) plot of the compressed laser beam from the *Salle Jaune* laser system, where a two crystal XPW is used to enhance the temporal contrast. The dashed plot represents the filtered curve with replicas removed.

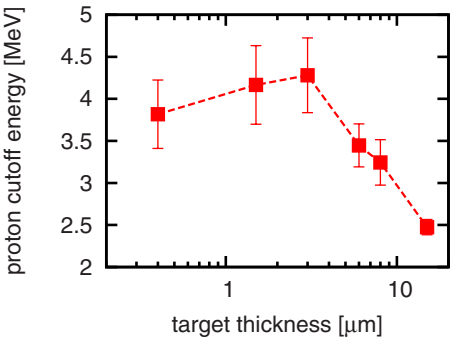


FIG. 2. (Color online) Proton cut-off energy for different target thicknesses with the fully compressed beam ($\tau_L$=30 fs). The optimum is observed between 1.5 and 3 $\mu$m. (Dashed lines are added to help visualization.)

*pliquée*. The laser pulse has a central wavelength of $\lambda$ =800 nm and a duration, at the maximum compression, of $\tau_L$=30 fs. The temporal contrast of the pulse is improved by a two-crystal Crossed Polarized Wave generation system [29] (XPW), which is inserted between the front-end of the Chirped Pulse Amplification (CPA) chain and the first amplification stage. The contrast of the output pulse, measured by $3\omega$ autocorrelator before injection in the amplification chain, is as high as $I_0/I_{\mathrm{ASE}}=10^{10}$; a small pedestal is observed starting from $t=-50$ ps before the pulse and rising to $I_0/10^8$ (Fig. 1). During the experiment shots, the contrast of the fully amplified beam is kept under control by a fast photomultiplier tube and a 7 GHz oscilloscope. No pedestal was ever observed above the measurable limits of $10^{-9}$ in dynamic and $t=-400$ ps in time. The phase front is corrected after compression by a deformable mirror and the beam focused down to a waist of 2.3 $\mu$m by an $f/3$ off-axis parabola. A total of 250 mJ (about 70% of the total on-target energy) is contained in the $1/e^2$ focal spot (measured) which results in a peak intensity, at maximum compression, of $I_0$ $=4\times10^{19}$ W/cm$^2$. The $p$-polarized beam impinges at 45° on thin aluminum targets. The different ion species accelerated from the target are collected and separated by a Thomson Parabola, and their spectra obtained from a Micro-Channel Plate (MCP) detector, imaged by a 16bit CCD camera. A 200 $\mu$m lead pinhole, 40 cm far from the interaction point, is used to collimate the analyzed beam. The diagnostic system has been validated with CR39 detectors. The use of a real-time proton diagnostic allows a statistical treatment of the data: each experimental point below is the averaged value of at least four different shots; error bars corresponds to the standard deviation of the set.

The proton cutoff energy is shown in Fig. 2 for different target thicknesses and a constant laser pulse duration of $\tau_L$ =30 fs. The proton signal is stable and reproducible for targets as thin as 0.4 $\mu$m; the highest energy is obtained for 3 $\mu$m thick targets.

The detailed behavior for different laser pulse durations is studied on thin, $D_{\mathrm{thin}}$=1.5 $\mu$m, and thick, $D_{\mathrm{Thick}}$=15 $\mu$m, targets. The pulse duration is varied between $\tau_{\mathrm{min}}$=30 fs and $\tau_{\mathrm{max}}$=700 fs by changing the separation between the gratings in the compressor. The measurements are repeated for both positive and negative chirp; the obtained pulse duration is calculated by numerical interpolation of the experimental calibration curve of the compressor. Figure 3 shows the proton cutoff energies obtained for the two targets. For $D_{\mathrm{thin}}$, the proton cut-off energy decreases monotonically as the peak intensity is lowered by stretching the pulse. The behavior for $D_{\mathrm{Thick}}$ is qualitatively different. At the maximum compression the observed proton energy is lower than what is observed for $D_{\mathrm{thin}}$. As the pulse is stretched, a slight increase in proton energy results in the occurrence of a weak maximum, indicating that a pulse in the range 150÷250 fs is more efficient than shorter ones. For $\tau_L>150$ fs, the proton beam from $D_{\mathrm{Thick}}$ is more energetic than the one from $D_{\mathrm{thin}}$.

A preliminar set of simulations is performed with the hydrodynamic code ESTHER [30] on Aluminum targets of the two thicknesses, in order to verify the effect of the small residual pedestal (see Fig. 1) on the target conditions. The simulations show the formation of a small preplasma, which reaches a density scalelength of $L\sim90$ nm on the illuminated surface, at the arrival of the main intensity peak. However in no case is any ionization or early expansion of the back surface observed, which confirms that no correlation between the target thickness and the interaction conditions is added by the presence of the residual pedestal.

In order to explain the experimental results, we have performed a set of simulations with the two-dimensional (2D) particle-in-cell (PIC) code CALDER [31]. A $\lambda$=800 nm laser

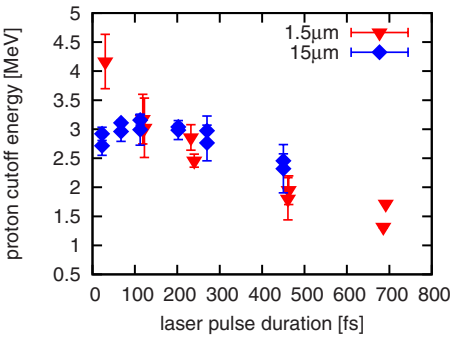


FIG. 3. (Color online) Proton cut-off energy for different laser pulse durations (at constant energy) on Aluminum targets of 1.5 and 15 $\mu$m.

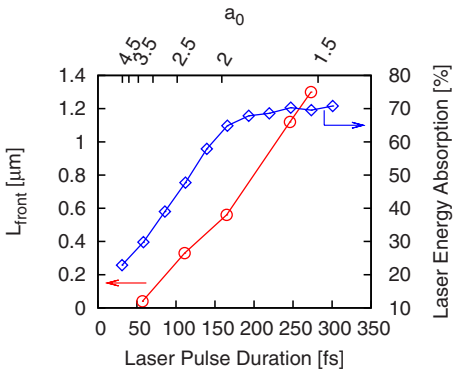


FIG. 4. (Color online) Simulated (2D PIC) values for the density gradient length on the illuminated surface *(circles)* and for the fraction of absorbed energy *(diamonds)* obtained with different pulse durations on the $D_{\mathrm{Thick}}$ target. The gradient length is measured by fitting the density profile with an exponential when the intensity peak arrives on the surface.

pulse, with spatial and temporal Gaussian profiles, is focused to a 5 $\mu$m spot. The total energy of the pulse is $E_L = 250$ mJ in the $1/e^2$ spot and it impinges under $p$ polarization at 45° on an homogeneous slab of fully ionized Hydrogen, at the density of $n_e = 50 n_c$ and at the initial temperature of 1 eV. The preplasma calculated with the hydro code is so small that we chose to ignore it in the PIC simulation setup. The intensity peak enters the simulation box at $t = 1.83\tau_L$, $\tau_L$ being the full width at half maximum duration of the laser pulse. In this way, the interaction of the rising front of the pulse is fully taken in account. The laser pulse duration is varied from 30 fs to 300 fs. The simulations have been run for the two thicknesses of 3 and 0.9 $\mu$m.

The PIC simulations show that the pulse duration plays a major role in laser absorption at the illuminated surface, as it impacts on both the hot electron temperature $T_{\mathrm{hot}}$ and the total absorbed energy. Figure 4 shows (blue diamonds) that the ratio of absorbed energy rises from ~20% to ~60% and then saturates to values of the order of ~70%. The leading edge of the longer pulses starts earlier to heat the surface, which results in the expansion of a preplasma; the gradient length that is present when the intensity peak interacts with the surface (red circles on the same figure) increases as the pulse is stretched. This behavior is qualitatively the same for $D_{\mathrm{thin}}$ and $D_{\mathrm{Thick}}$.

For the shortest pulse ($\tau_L = 30$ fs, $a_0 = eA/mc = 4.6$), a hot electron temperature $T_{\mathrm{hot}} = 0.24$ MeV is observed (Fig. 5); the electron temperature increases as the pulse gets longer, illustrating that the lower laser field amplitude is compensated by an improved coupling with the plasma. The maximum temperature is reached for pulse durations between 100 and 150 fs. After the maximum is reached, the temperature decreases, as the normalized field amplitude approaches to $a_0 = 1$ (relativistic limit). Figure 5 shows that the heating process is similar for the two target thicknesses, and does not exhibit any effect of electron recirculation on electron temperature for the thinner target.

The dependence of the acceleration conditions on target thickness is made evident by the hot electron density on the rear (accelerating) surface. As laser intensity during the leading edge of the pulse increases over $\sim 10^{17}$ W/cm$^2$, important electron heating starts. Fast electrons generated on the front surface travel to the back side and start driving the expansion, resulting in the formation of a density gradient. Simulations show that the gradient length $L_{\mathrm{back}}$ of the plasma on the rear surface (see circles in Fig. 6) is similar in the two cases, consistent with the similar temperatures measured in Fig. 5. By looking at the hot electron density (crosses on the same plot) it is evident that the thinner target reaches a higher density of hot electrons than the thicker one. This is in agreement with the picture of hot electrons experiencing less dilution in thinner targets than in thicker ones [33].

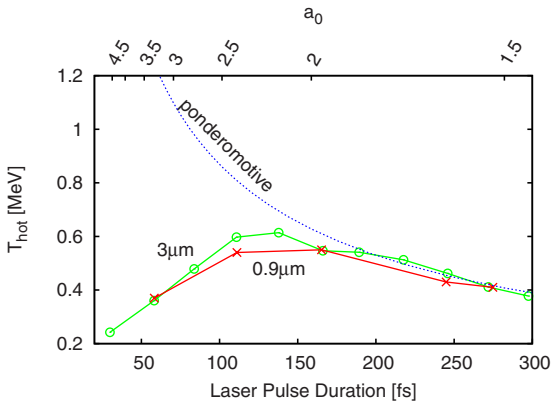


FIG. 5. (Color online) Hot electron temperature (simulation) for the 3 and 0.9 $\mu$m targets and different pulse durations. The ponderomotive temperature [32] is added for comparison (dashed line).

According to [15], two separate regimes of proton acceleration are recognized during the expansion of the plasma. In the first regime, for $\lambda_D > L_{\mathrm{back}}$, the TNSA accelerating field scales as $\propto \sqrt{n_{\mathrm{hot}} T_{\mathrm{hot}}}$, $\lambda_D$ being the hot electron Debye length and $n_{\mathrm{hot}}$ the hot electron density on the rear surface. From Figs. 5 and 6, for $t < 100$ fs ($a_0 > 2.2$), an increase in pulse duration increases both the hot electron number and temperature, which corresponds, in the $\sqrt{n_{\mathrm{hot}} T_{\mathrm{hot}}}$ regime, to an increase in the proton energy. As the maximum $T_{\mathrm{hot}}$ is reached, the proton energy is expected to decrease: in fact the electron temperature falls down, whereas the energy absorption (Fig. 4) saturates. When the inequality changes, $\lambda_D \ll L_{\mathrm{back}}$ the ac-

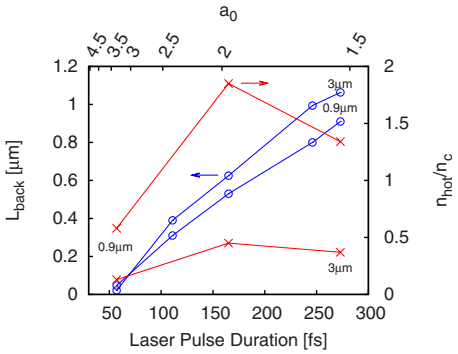


FIG. 6. (Color online) Density scale length on the back (nonilluminated) surface (*circles*). Hot electron density at the back surface (*crosses*). Values are measured when the intensity peak arrives on the front surface.

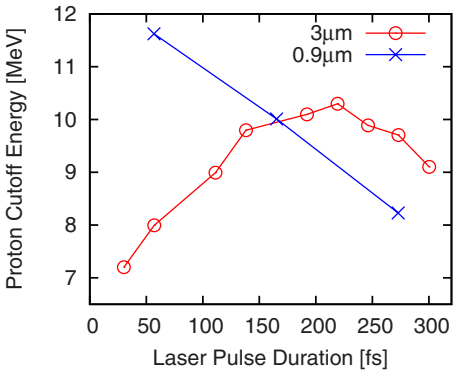


FIG. 7. (Color online) Comparison between the maximum simulated proton energy for thin (0.9 $\mu$m) and thick (3 $\mu$m) targets.

celerating field scales as $\propto T_{\mathrm{hot}}/L_{\mathrm{back}}$. This change in dependence adds a correlation between the conditions of acceleration and the thickness of the target. In fact (Fig. 6), while the evolution of $L_{\mathrm{back}}$ with the pulse duration is comparable for the two thicknesses, the hot electron density is larger for thinner target and the hot electron Debye length of the thicker target is therefore larger. Starting from a $\lambda_D > L_{\mathrm{back}}$ regime at short pulse durations, the thinner target will more rapidly evolve to a gradient-dominated expansion. Indeed, the simulations show that for $D_{\mathrm{Thick}}$ the second regime is reached at $\tau_L \sim 200$ fs, and that the same should happen for $D_{\mathrm{thin}}$ at $\tau_L < 30$ fs. Once the $\lambda_D \ll L_{\mathrm{back}}$ regime is reached, the proton energy is governed by the density gradient on the rear surface, which worsens the acceleration condition as $\tau_L$ keeps increasing. Figure 7 shows the simulated proton energy, which clarify the overall effect. On $D_{\mathrm{Thick}}$ the energy increase is slowed down for $\tau_L$ between 130 and 220 fs, and starts decreasing for longer durations. For the thinner target, the accelerating field is instead completely governed by the expansion of the rear surface, in the $\lambda_D \ll L_{\mathrm{back}}$ regime. The behavior observed in the simulations qualitatively reproduces the experimental data presented in Fig. 3. In particular, the simulations show that for a laser pulse duration $\tau_L > 150$ fs, the protons accelerated from the thicker target are more energetic than those from the thinner one, in agreement with the experiment (Fig. 3). To understand why a quantitative agreement is not observed, it is important to underline that the simulation target (material, thickness, density) is notably different from what was used in the experiments. This is particularly important when considering that the transition between the two regimes is regulated by the local electron density on the rear surface, thus depending on the electron transport through the target.

In conclusion we reported the behavior of a laser proton accelerator for different pulse durations in conjunction with two different target thicknesses. For constant laser energy, the proton cutoff depends on the balance between the increased efficiency of the laser-plasma coupling and the maximum obtainable electron temperature. The ratio between the rear density gradient and the Debye length sets the proton acceleration regime, with an accelerating field scaling either as $T_{\mathrm{hot}}/L_{\mathrm{back}}$ for $\lambda_D \ll L_{\mathrm{back}}$ or as $\sqrt{n_{\mathrm{hot}} T_{\mathrm{hot}}}$ for $\lambda_D > L_{\mathrm{back}}$. We believe that our experimental measurements shed light on a correlation among the interaction parameters (duration of the pulse and thickness of the target) that was not completely clarified before. Our observations are also supported by PIC simulations, evidencing unexpected variations in absorption and temperature with intensity. It is important to underline that these effects can be observed only on laser systems where the lack of pedestal provides sufficiently clean interaction conditions with dense targets. Under these conditions, absorption and temperature are found to be decreasing functions of intensity, at constant laser energy. This experimental work suggests that for an optimal acceleration of ions, the experimental parameters should fall within the $\sqrt{n_e T_e}$ regime, where a pre-existent preplasma could be used to enhance the energy absorption on a thicker target and increase the proton cut-off energy [14,34].

This work was partially supported by the ANR under Project No. ANR-08-NT08-1-380251. The authors wish to thank P. Combis for help with the ESTHER code.

[1] E. L. Clark *et al.*, Phys. Rev. Lett. **84**, 670 (2000).
[2] R. A. Snavely *et al.*, Phys. Rev. Lett. **85**, 2945 (2000).
[3] S. P. Hatchett *et al.*, Phys. Plasmas **7**, 2076 (2000).
[4] M. Borghesi, A. J. Mackinnon, D. H. Campbell, D. G. Hicks, S. Kar, P. K. Patel, D. Price, L. Romagnani, A. Schiavi, and O. Willi, Phys. Rev. Lett. **92**, 055003 (2004).
[5] T. E. Cowan *et al.*, Phys. Rev. Lett. **92**, 204801 (2004).
[6] A. Gurevich, D. Anderson, and H. Wilhelmsson, Phys. Rev. Lett. **42**, 769 (1979).
[7] M. A. True, J. R. Albritton, and E. A. Williams, Phys. Fluids **24**, 1885 (1981).
[8] A. Pukhov, Phys. Rev. Lett. **86**, 3562 (2001).
[9] J. Fuchs *et al.*, Phys. Rev. Lett. **94**, 045004 (2005).
[10] F. Brunel, Phys. Rev. Lett. **59**, 52 (1987).
[11] W. L. Kruer and K. Estabrook, Phys. Fluids **28**, 430 (1985).
[12] J. P. Freidberg, R. W. Mitchell, R. L. Morse, and L. I. Rudsinski, Phys. Rev. Lett. **28**, 795 (1972).
[13] A. A. Andreev, R. Sonobe, S. Kawata, S. Miyazaki, K. Sakai, K. Miyauchi, T. Kikuchi, K. Platonov, and K. Nemoto, Plasma Phys. Controlled Fusion **48**, 1605 (2006).
[14] R. Nuter, L. Gremillet, P. Combis, M. Drouin, E. Lefebvre, A. Flacco, and V. Malka, J. Appl. Phys. **104**, 103307 (2008).
[15] T. Grismayer and P. Mora, Phys. Plasmas **13**, 032103 (2006).
[16] A. J. Mackinnon, M. Borghesi, S. Hatchett, M. H. Key, P. K. Patel, H. Campbell, A. Schiavi, R. Snavely, S. C. Wilks, and O. Willi, Phys. Rev. Lett. **86**, 1769 (2001).
[17] J. Fuchs *et al.*, Phys. Rev. Lett. **99**, 015002 (2007).
[18] M. Kaluza, J. Schreiber, M. I. K. Santala, G. D. Tsakiris, K. Eidmann, J. Meyer-ter-Vehn, and K. J. Witte, Phys. Rev. Lett. **93**, 045003 (2004).
[19] T. Ceccotti, A. Lévy, H. Popescu, F. Réau, P. D'Oliveira, P. Monot, J. P. Geindre, E. Lefebvre, and P. Martin, Phys. Rev.

Lett. **99**, 185002 (2007).
[20] P. Mora, Phys. Rev. Lett. **90**, 185002 (2003).
[21] P. Mora, Phys. Rev. E **72**, 056401 (2005).
[22] J. Schreiber, F. Bell, F. Grüner, U. Schramm, M. Geissler, M. Schnurer, S. Ter-Avetisyan, B. M. Hegelich, J. Cobble, E. Brambrink, J. Fuchs, P. Audebert, and D. Habs, Phys. Rev. Lett. **97**, 045005 (2006).
[23] M. Carrié, E. Lefebvre, A. Flacco, and V. Malka, Phys. Plasmas **16**, 053105 (2009).
[24] A. J. Mackinnon, Y. Sentoku, P. K. Patel, D. W. Price, S. Hatchett, M. H. Key, C. Andersen, R. Snavely, and R. R. Freeman, Phys. Rev. Lett. **88**, 215006 (2002).
[25] Y. Oishi, T. Nayuki, T. Fujii, Y. Takizawa, and X. Wang, Phys. Plasmas **12**, 073102 (2005).
[26] L. Robson *et al.*, Nat. Phys. **3**, 58 (2007).
[27] J. Fuchs *et al.*, Nat. Phys. **2**, 48 (2006).
[28] D. Neely, P. Foster, A. Robinson, F. Lindau, O. Lundh, A. Persson, C. G. Wahlström, and P. McKenna, Appl. Phys. Lett. **89**, 021502 (2006).
[29] A. Jullien, O. Albert, G. Chériaux, J. Etchepare, S. Kourtev, N. Minkovsky, and S. M. Saltiel, Opt. Express **14**, 2760 (2006).
[30] S. Jacquemot, L. Bonnet, and A. Decoster, Laser Interaction with Matter Institute of Physics Conference Series, 1995 (unpublished), Vol. 140, p. 193.
[31] E. Lefebvre *et al.*, Nucl. Fusion **43**, 629 (2003).
[32] S. C. Wilks, W. L. Kruer, M. Tabak, and A. B. Langdon, Phys. Rev. Lett. **69**, 1383 (1992).
[33] J. J. Santos, A. Debayle, P. Nicolaï, V. Tikhonchuk, M. Manclossi, D. Batani, A. Guemnie-Tafo, J. Faure, V. Malka, and J. J. Honrubia, Phys. Plasmas **14**, 103107 (2007).
[34] A. Flacco, A. Guemnie-Tafo, R. Nuter, M. Veltcheva, D. Batani, E. Lefebvre, and V. Malka, J. Appl. Phys. **104**, 103304 (2008).